Preparation of concentrated multilayer graphene dispersions and TiO2-graphene composites for enhanced hydrogen production

Preparation of Concentrated Multilayer Graphene Dispersions and TiO$_2$-graphene Composites for Enhanced Hydrogen Production

Rei Mizuno, Reina Tsuchihashi, Shingo Furukawa, Hitomi Takano, Mai Takase, Yoshikazu Kuga, Shinya Yamanaka[*]

Course of Applied Chemistry, Muroran Institute of Technology, Mizumoto-cho 27-1, Muroran 050-8585, Japan

[*]Corresponding author. Tel: +81 143 46 5747. Fax: +81 143 46 5701.

E-mail address: syama@mmm.muroran-it.ac.jp (S. Yamanaka)

Abstract:

Photocatalytic hydrogen (H_2) production is an attractive hydrogen production technology. It is initiated by charge-separation in titanium (IV) dioxide (TiO_2) upon photoexcitation. Electrons reduce water to generate H_2 while holes oxidize hydroxide to generate hydroxyl radicals. TiO_2 is widely used because it is inexpensive, chemically stable, nontoxic, and environmentally friendly. The activity of TiO_2 is limited, but adding a supporting noble metal nanoparticle such as platinum greatly enhances it. Due to resource risks and cost issues, we consider using graphene as an alternative to noble metal nanoparticles. Herein we report a new method to prepare a concentrated multilayer graphene solution and hydrogen production from an aqueous methanol solution. When we used graphene with different sheet sizes or improved the aggregation of TiO_2 (TIO-9), the H_2 evolution rate is 1.6 times higher than that of pristine TIO-9. The contact state and the dispersed state of graphene and TiO_2 play important roles in improving the activity.

1. Introduction

Hydrogen produced via water-splitting technology is considered to be a clean and renewable energy source. Economical hydrogen production with a small environmental load is indispensable for widespread fuel cells. Currently, the most common hydrogen production method removes hydrogen from fossil fuels such as petroleum and natural gas. Merits of this method include economical and energy efficient production of large quantities of hydrogen in a short time. The major drawbacks are the consumption of fossil fuels and the discharge of carbon dioxide. Consequently, clean and efficient production methods are necessary to realize a full-fledged hydrogen society.

Great attention has been focused on photocatalytic hydrogen production. It is initiated by charge separation in TiO_2 upon photoexcitation. Electrons reduce water to generate H_2 while holes oxidize hydroxide to generate hydroxyl radicals. TiO_2 is widely used as a photocatalyst [1-6] because it is low cost, highly stable, nontoxic, and environmentally friendly [7-14]. Many studies have employed TiO_2-based photocatalysts. The activity of pure TiO_2 is limited, but the activity is greatly improved by supporting noble metal nanoparticles such as Pt on TiO_2 [15]. The characteristics of TiO_2-carbon composites have been extensively studied. The most popular two-dimensional graphite carbon material is graphene, which possesses excellent properties [16,17].

Graphene is one atomic layer thick, and has both a high electron mobility and a high theoretical specific surface area, making it a useful alternative to Pt. Recently, the addition of graphene has been demonstrated as an effective method to improve the photocatalytic and electrochemical performance [18-25]. Excited electrons can be transferred from the conduction band (CB) of TiO_2 to the surface of graphene, improving the separation of the electron–hole pairs and preventing their recombination. The band-gap energy decreases, shifting the absorption threshold to the visible light region and allowing solar energy to be harnessed.

Since the first graphene isolation method was reported in 2004 [26], research on manufacturing methods and graphene applications has rapidly advanced [27-29]. To date, various manufacturing methods have been proposed, and some are economical. However, few of these can be applied from the viewpoint of mass synthesis. The method of peeling graphite in the liquid phase has attracted attention because the reaction area is remarkably large and the equipment cost is low. To stably disperse the separated graphene, a high concentration graphene dispersion can be obtained by exfoliation to a polar solvent N-methylpyrrolidone (NMP) or ionic liquid [30-32], but its use is limited because it has a high boiling point and is expensive.

A liquid phase separation using a simple solvent and a surfactant in water is highly

desired [33]. Herein we improve the liquid phase exfoliation to obtain a high concentration graphene dispersion in a short time by adding ceramics beads to water and a surfactant. This study attempts to enhance the activity of graphene–TiO_2 composites using graphene prepared by this method.

2. Photocatalytic water splitting

The electronic structure of a semiconductor plays a key role in semiconductor photocatalysis. The photocatalyst is a semiconductor, which is composed of a valence band (VB) and CB. The energy difference between these two levels is the band gap energy. Without excitation, both electrons and holes are in the VB. The semiconductor itself becomes a high-energy state by receiving light energy and emitting electrons on the surface hit by light. When a semiconductor is excited by photons with an energy equal or higher than the band gap energy level, electrons transfer is promoted from the VB to CB.

The photogenerated electrons and holes can recombine in the bulk or on surface of the semiconductor within a very short time. The absorbed light energy is converted into thermal energy, but is not involved in a chemical reaction. Electrons and holes that migrate to the surface of the semiconductor without recombination can respectively reduce and oxidize the reactants adsorbed by the semiconductor. In general, visible light

(wavelength 400–800 nm) covering half of the solar energy spectrum is thermodynamically suitable for water decomposition.

The mechanism is explained by the fact that the lower end potential of the TiO_2 CB is more negative than the oxidation reduction potential of H^+/H_2 and the upper end potential of the VB is more positive than the oxidation potential (1.23 V) of water. However, the real problems are the development of semiconductors that absorb longer wavelengths and the water disintegration capability. During the water splitting reaction, hole recombination is frequently observed. Thus, the addition of a scavenger reagent like methanol, ethanol, or sulfide/sulfite is necessary to enhance the photocatalytic process [35-39].

In this case, the reaction is not pure water splitting. In the presence of alcohol, the energy required for water splitting tends to be lower as described by Kawai and Chen [39,40] through the following overall reaction: $CH_3OH_{(l)} + H_2O_{(l)} \leftrightarrow CO_{(g)} + 3H_{2(g)}\Delta G° = 16.1$ kJ/mol. Since methanol has a low boiling point and a high H/C ratio, it is widely accepted as an excellent raw material for high-purity hydrogen. Methanol in a water–alcohol mixture is a satisfactory hole-capturing agent, resulting in a better efficiency than other compounds. Methanol decomposition can achieve two objectives. First, it increases hydrogen production as a result of methanol decomposition occurring

during the process. Second, the decomposition products decompose into less toxic substances.

3. Experimental

3.1 Preparation of a graphene dispersion

A mono/multilayer graphene dispersion was prepared via our original method. In a typical experiment, 15 g distilled water, 2.25 g natural graphite (Brazil, mean size of 18 μm), and 0.12 g TritonX-100 (Alfa Aeser) as a surfactant were placed into a 250 ml screw tube. As the first step to propose a new catalyst, we investigated the effects of the sheet size of the graphene and dispersibility of graphene and TiO_2 on the catalytic activity in this study. As the result, we selected the conditions as follows. Zirconia beads (140 g, 3 mm; Nikkato) or alumina beads (3 mm; AS ONE) were put into a mixed suspension and irradiated with ultrasonic waves (37 kHz for 3 h in zirconia, 5 h in alumina) to prepare a dispersion. The obtained suspension was centrifuged at 20 °C and 22,140 G (15,000 rpm) for 30 min. The supernatant was divided by size using suction filtration and a membrane filter with a 5-μm pore size.

3.2 Characterization of graphene dispersion

The concentration of the dispersion was measured by a UV–Vis spectrophotometer

(Shimadzu, UV-1800). Using a membrane filter with a 0.22-μm pore size, the dispersion was suction-filtered. Then the filter was dried at 90 °C for 1 h. The concentration of the reference dispersion was calculated by measuring the mass of the membrane filter before and after filtration. The calibration curve was prepared by diluting the reference dispersion, measuring the absorbance at 660 nm [41], and plotting the dispersion concentration as a function of the absorbance. The correlation coefficient of the calibration curve was ≥ 0.99, and the concentration was calculated using this calibration curve.

The prepared graphene was analyzed using a transmission electron microscope (TEM, JEOL, JFM-2100F) and a Raman spectroscope (Renishaw 2000; 50× objective lens; ~1-μm spot diameter, λ_{ex}=785 nm).

3.3 Graphene–TiO$_2$ photocatalytic reaction

The graphene–TiO$_2$ composite photocatalyst was prepared by stirring. TiO$_2$ (50 mg), 0.04 mg graphene (0.08 wt% based on TiO$_2$), and 20 ml ultrapure water were stirred and freeze-dried. The graphene–TiO$_2$ photocatalyst (50 mg) was dispersed in a methanol 50% aqueous solution. A 400-W high-pressure mercury lamp was used as the light source. The H$_2$ evolution was analyzed using a gas chromatograph (GC-8AIT; Shimadzu).

TIO-9 was mainly used in this study because the TIO-9 showed the highest activity when we used pristine TiO_2 particles (see Table 3, and Fig. 3a).

4. Results and discussions

Table 1 compares the graphene dispersion concentrations prepared in recent years. **Table 2** summarizes our preparation conditions and graphene characteristics. Comparisons with previous studies are difficult due to the differences in the gravity of centrifugation. We realize a similar concentration (0.139 or 0.333 mg/ml) as Ref. 33 (1.0 mg/ml), but our centrifuge condition is 44 times higher. Hence, our method provides a relatively high concentration dispersion.

Figure 1 shows the TEM image of graphene made of zirconia beads (a) and alumina beads (b). In both cases, mono and multilayer graphene is observed, but the mean sheet size differs. The mean sheet size is (a) 0.5 μm and (b) 0.07 μm (Table 2). Because the densities of zirconia and alumina beads were 6.0 and 3.8 g/cm^3, respectively, the physical movement of the beads may differ during sonication, leading to a complex mechanism that involves grinding and peeling of raw graphite.

The Raman spectrum for a graphene dispersion prepared using zirconia beads has a G band (1590 cm^{-1}), indicating a carbon material with sp2 bonding (**Fig. 2**). Additionally,

Table 1 Recently fabricated graphene dispersion concentrations and conditions.

Solvent	Additive	Centrifuge condition	Concentration [mg/ml]	Reference
NMP	–	1000 rpm, 30 min	0.1	31
NMP	–	4000 rpm, 30 min	2.21	30
Ion liquid	–	4000 rpm, 30 min	5.33	32
Ethanol	copolymers	Kept for 7 days	1.8	34
Water	P-123	500 G, 5 min	1.0	33

Table 2 Conditions and characteristics of graphene prepared in this study.

Beads	Irradiation time [h]	Concentration [mg/ml]	Size* [μm]	H_2 evolution [μmol/g·h]
Zirconia	3	0.139	0.50	0.386
Alumina	5	0.333	0.07	0.770

* Mean size is measured for 50 sheets from TEM images.

the G' band peak (2600 cm^{-1}) due to monolayer graphene is observed. To investigate the presence or absence of defects in graphene, we investigated the type of defects in graphene using the method of Eckmann et al. [42]. They suggested that the defect type can be distinguished by the intensity ratio of the D-band (2700 cm^{-1}) to the D' band (1620 cm^{-1}) in the Raman spectrum. They found that the ID/ID' ratio depends on the kind of defect. An sp3 defect was ~13, while a point defect was ~7. However, the Raman spectrum of this graphene is not attributed to sp3 or a point defect. The $I_D/I_{D'}$ in this experiment is 3.1, which approximates an edge defect ($I_D/I_{D'}$=3.5). Consequently, the graphene in this experiment mainly has edge defects.
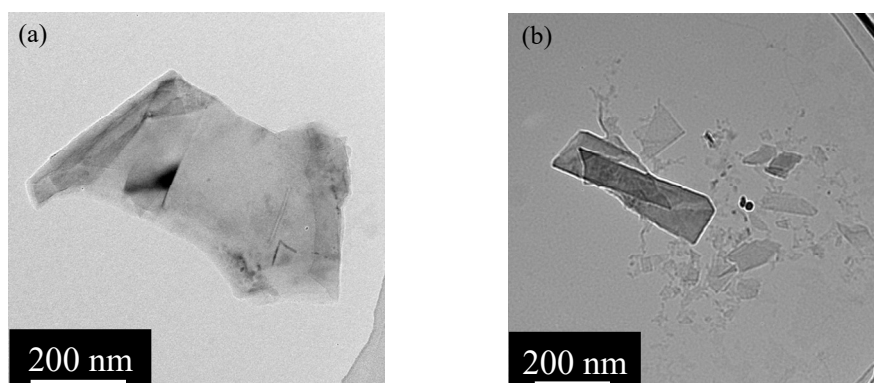

Fig. 1 TEM images of mono and multilayer graphene comprised of (a) zirconia and (b) alumina beads.
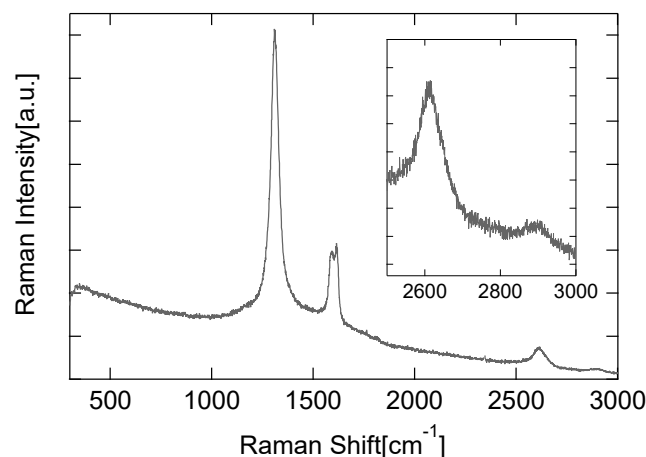
Fig. 2 Raman spectrum for a graphene dispersion prepared with zirconia beads.

TiO$_2$ catalysts provided by the Catalysis Society of Japan (TIO-2, TIO-4, TIO-8, TIO-9, and TIO12) were used as references. **Table 3** lists the physical properties, and the H$_2$ evolution is shown in **Fig. 3a**. The addition of graphene improves the activities of TIO-4, TIO-8, and TIO-12. Graphene addition has a minimal impact on TIO-2 but decreases the activity of TIO-9. Since the TIO-9 activity is the only one negatively impacted, TIO-9 has the highest activity with pristine TiO$_2$ particles. The decrease in activity is attributed to the contact state between graphene and TiO$_2$. As observed by TEM, TIO-9 agglomerates. The sheet size of the multilayered graphene is large and inhomogeneous (**Fig. 3b**). We attempted to use thin and small graphene to improve this inhomogeneous state. Using graphene (Fig. 1b) made of alumina beads improves the activity (Table 2).

Table 3 Properties of TiO$_2$.

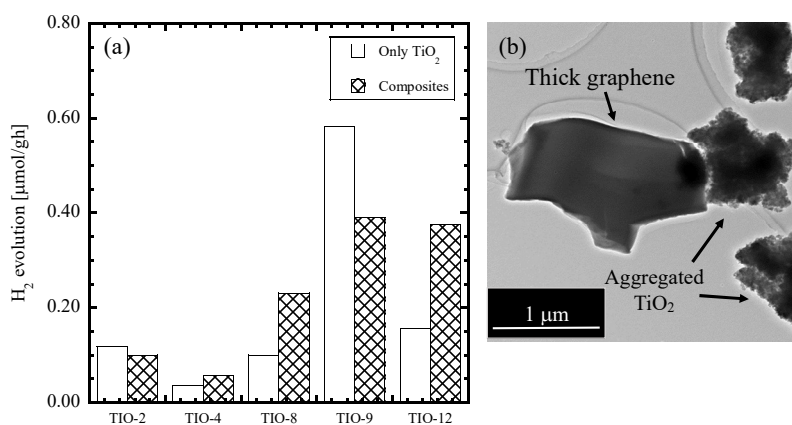|	TIO-2	TIO-4	TIO-8	TIO-9	TIO-12
Primary particle size	0.4 mm	~ 21 nm		8–11 nm	~ 6 nm
Specific surface area [m^2/g]	18	50±15	338	290–310	290
Method	sulfate	chlorine	–	sulfate	–
Crystal structure	anatase	anatase /rutile	anatase	anatase	anatase

Fig. 3 (a) H$_2$ evolution for each photocatalyst and (b) TEM image of the graphene–TIO-9 composite.

Because the TIO-9 showed the highest activity when we used pristine TiO_2 particles, the effects of the amount of added graphene and graphene size on the maximum activity were investigated using TIO-9. The graphene loading amount was 0.08 wt%, which yields the maximum activity (**Fig. 4a**). The graphene size was divided using a membrane filter with a suction filtration pore size of 10, 8, 5, 1.2, or 0.1 μm. The amount of H_2 evolution is shown in **Fig. 4b**. Although the highest activity is obtained at ≤ 5 μm, TEM reveals that graphene is more covered with TiO_2 than expected due to small and thin graphene. This suggests that the light irradiation to graphene is insufficient. **Figure 4c** shows the TEM image of the composite catalyst (0.08 wt%, < 5 μm). From the viewpoint of the electron transfer, Kamat reported an ideal surface or contact state between TiO_2 and graphene [43]. The above results show that the catalytic activity is affected by the contact state of the TIO-9 and the graphene (**Fig. 5a**).

To improve the agglomeration of TIO-9, as seen in the TEM images in Fig. 3b and Fig. 4c, the amount of added TIO-9 is reduced from 50 mg to 5 mg. **Table 4** indicates the H_2 evolution. The activity per unit weight is improved, and the maximum activity (0.95 μmol/g·h) is obtained at 5 mg TIO-9. This value is 1.6 times higher than that of pristine TIO-9. The XRD and UV-DRS spectra for the graphene–TIO-9 composites (corresponds to Fig. 3b, Fig. 4c, and Fig. 5b, respectively.) were shown in **Figs. S1**, and **S2** (see
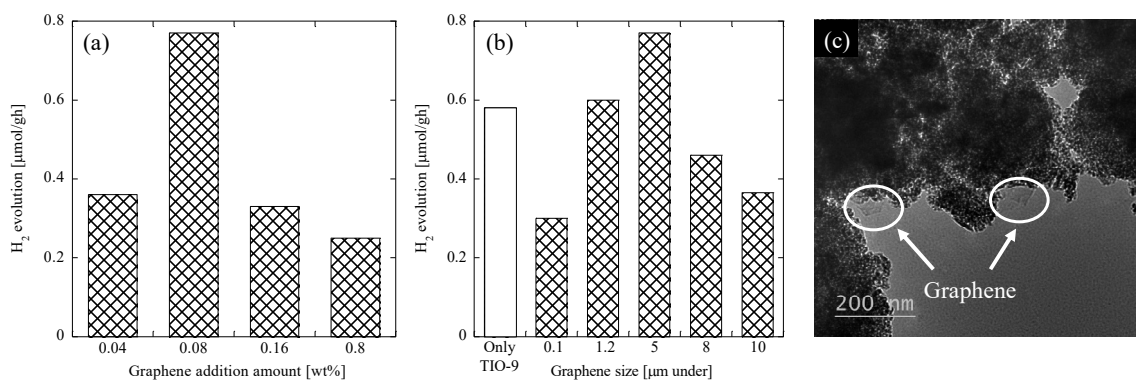
Fig. 4 Effects of (a) the additional amount and (b) sheet size of graphene on the catalytic activity of the graphene–TIO-9 composite. (c) TEM image of the composite (0.08 wt%, ≤ 5 μm).

supporting information). **Figure 5b** shows the TEM image of the composite photocatalyst when the additional amount of TIO-9 is close to the ideal dispersion state described above (Fig. 5a). In addition, the same tendency is observed for activity with only TIO-9, suggesting that the dispersibility of TiO_2 is also important. Therefore, when the contact state and dispersibility of graphene and TiO_2 are closer to the ideal state, the activity improves.
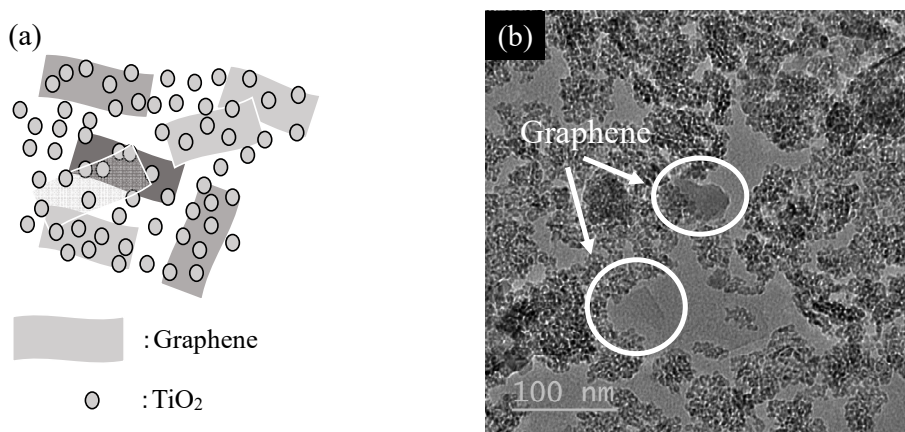
Fig. 5 (a) Ideal contact state of the graphene–TIO-9 composite. (b) Improved activity due to the dispersion of TIO-9.

Table 4 Improvement of activity by reducing the additional amount of TIO-9.

TIO-9	Graphene	H_2 evolution [μmol/g·h]
50 mg	0.04 mg	0.40
5 mg	0.04 mg	0.95

5. Conclusion

Adding ceramics beads to water and a surfactant not only improves the liquid phase

exfoliation but also realizes a new method to prepare high concentrations of mono and multilayer graphene dispersions in a short time. The ability of graphene to enhance the activity of the graphene–TiO$_2$ (TIO-9) composite photocatalyst was evaluated. Adding 0.08 wt% of graphene to TIO-9 decreases the activity, whereas using graphene with different sheet sizes or improving the aggregation of TIO-9 enhances the activity to about 1.6 times higher than the H$_2$ evolution amount using only the initial TIO-9. These results indicate that the contact and dispersed states of graphene and TiO$_2$ are important to improve the activity.

References

[1] T. Leshuk, R. Parviz, P. Everett, H. Krishnakumar, R. A. Varin, F. Gu, Photocatalytic activity of hydrogenated TiO$_2$, ACS Appl. Mater. Interfaces 2013; 5 (6): 1892–1895.

[2] A. Natoli, A. Cabeza, Á. G. Torre, M. A. G. Aranda, I. Santacruz, H. Hintzen, Colloidal processing of microporous TiO$_2$ materials for photocatalytic water treatment, J. Am. Ceram. Soc. 2012; 95 (2): 502-508.

[3] X. Pan, Y. Zhao, S. Liu, C. L. Korzeniewski, S. Wang, Z. Fan, Comparing graphene-TiO$_2$ nanowire and graphene-TiO$_2$ nanoparticle composite photocatalysts,

ACS Appl. Mater. Interfaces 2012; 4 (8): 3944-3950.

[4] J. N. T. Bak, M. Rekas, C. C. Sorrell, Photo-electrochemical hydrogen generation from water using solar energy. Materials-related aspects, Int. J. Hydrog. Energy 2002; 27: 991-1022.

[5] M. Ni, M. K. H. Leung, D. Y. C. Leung, K. Sumathy, A review and recent developments in photocatalytic water-splitting using TiO_2 for hydrogen production, Renew. Sust. Energ. Rev. 2007; 11 (3): 401-425.

[6] X. Chen, S. S Mao, Titanium dioxide nanomaterials: synthesis, properties, modifications, and applications, Chem. Rev. 2007; 107 (7): 2891-2959.

[7] M. R. Hoffmann, S. T. Martin, W. Choi, D. W. Bahnemann, Environmental applications of semiconductor photocatalysis, Chem. Rev. 1995; 95 (1): 69-96.

[8] M. A. Fox, M. Dulay, Heterogeneous photocatalysis, Chem. Rev. 1993; 93 (1): 341-357.

[9] P. V. Kamat, Photochemistry on nonreactive and reactive (semiconductor) surfaces, Chem. Rev. 1993; 93 (1): 207-300.

[10] A. L. Linsebigler, C. Lu, J. T. Yates Jr., Photocatalysis on TiO_2 surfaces: principles, mechanisms, and selected results, Chem. Rev. 1995; 95 (3): 735–758.

[11] O. Carp, C. L. Huisman, A. Reller, Photoinduced reactivity of titanium dioxide, Prog. Solid State Chem. 2004; 32 (1–2): 33–177.

[12] U. I. Gaya, A. H. Abdullah, Heterogeneous photocatalytic degradation of organic contaminants over titanium dioxide: a review of fundamentals, progress and problems, J. Photochem. Photobiol. 2008; C 9 (1): 1–12.

[13] G. Kenanakis, D. Vernardou, A. Dalamagkas, N. Katsarakis, Photocatalytic and electrooxidation properties of TiO_2 thin films deposited by sol–gel, 2015; Catal. Today 240: 146–152.

[14] M. N. Abellán, J. Giménez, S. Esplugas, Photocatalytic degradation of antibiotics: the case of sulfamethoxazole and trimethoprim, Catal. Today 2009; 144 (1–2): 131–136.

[15] E. Formo, E. Lee, D. Campbell, Y. Xia, Functionalization of electrospun TiO_2 nanofibers with Pt nanoparticles and nanowires for catalytic applications, Nano Lett. 2008; 8 (2): 668–672.

[16] X. Yu, W. Zhang, P. Zhang, Z. Su, Fabrication technologies and sensing applications of graphene-based composite films: advances and challenges, Biosens. Bioelectron. 2017; 89 (1): 72–84.

[17] X. Zhao, Y. Li, J. Wang, Z. Ouyang, J. Li, G. Wei, Z. Su, Interactive oxidation reduction reaction for the in situ synthesis of graphene-phenol formaldehyde composites with enhanced properties, ACS Appl. Mater. Interfaces 2014; 6 (6): 4254–4263.

[18] Q. Xiang, J. Yu, M. Jaroniec, Enhanced photocatalytic H_2-production activity of graphene-modified titania nanosheets, Nanoscale 2011; 3: 3670–3678.

[19] W. Wang, J. Yu, Q. Xiang, B. Cheng, Enhanced photocatalytic activity ofhierarchical macro/mesoporous TiO_2–graphene composites for photodegradation of acetone in air, Appl. Catal. B: Environ. 2012; 119–120: 109–116.

[20] J. Ryu, S. Kim, H.I. Kim, E.-H. Jo, Y. K. Kim, M. Kim, H. D. Jang, Self-assembled TiO_2 agglomerates hybridized with reduced-graphene oxide: a high-performance hybrid photocatalyst for solar energy conversion, Chem. Eng. J. 2015; 262: 409–416.

[21] X. Li, J. Yu, J. Low, Y. Fang, J. Xiao, X. Chen, Engineering heterogeneous semiconductors for solar water splitting, J. Mater. Chem. A 2015; 3: 2485-2534.

[22] J. Feng, Qun Li, J. Cai, T. Yang, J. Chen, X. Hou, Electrochemical detection mechanism of dopamine and uric acid on titanium nitride-reduced graphene oxide composite with and without ascorbic acid, Sens. actuators. B Chem. 2019; 298: 126872.

[23] N. Thangavel, S. Bellamkonda, A. D. Arulraj, G. R. Rao, B. Neppolian, Visible light induced efficient hydrogen production through semiconductor–conductor– semiconductor (S–C–S) interfaces formed between g-C_3N_4 and rGO/Fe_2O_3 core–shell composites, Catal. Sci. Technol. 2018; 8(19): 5081-5090.

[24] S. Bellamkonda, N. Thangavel, H. Y. Hafeez, B. Neppolian, G. R. Rao, Highly active and stable multi-walled carbon nanotubes-graphene-TiO_2 nanohybrid: An efficient non-noble metal photocatalyst for water splitting, Catal. Today 2019; 321-322: 120-127.

[25] Z. Fanga , Q. Lia , L. Sub , J. Chenc , K.-C. Choua, X. Hou, Efficient synergy of photocatalysis and adsorption of hexavalent chromium and rhodamine B over Al$_4$SiC$_4$/rGO hybrid photocatalyst under visible-light irradiation, Appl. Catal. B-Environ. 2019; 241: 548-560.

[26] K. S. Novoselov, V. I. Fal'ko, L. Colombo, P. R. Gellert, M. G. Schwab, K. Kim, A roadmap for graphene, Nature 2012; 490: 192-200.

[27] W. Norimatsu and M. Kusunoki, Growth of graphene from SiC{0001}surfaces and its mechanisms, Semicond. Sci. Technol. 2014; 29: 064009.

[28] J. N. Coleman, M. Lotya, A. O'Neill, S. D. Bergin, P. L. King, U. Khan, K. Young, A. Gaucher, S. De, R. J. Smith, I. V. Shvets, S. K. Arora, G. Stanton, H. Y. Kim, K. Lee, G. T. Kim, G. S. Duesberg, T. Jallam, J. J. Boland, J. J. Wang, J. F. Donegan, J. C. Grunlan, G. Moriarty, A. Shmeliov, R. J. Nicholls, J. M. Perkins, E. M. Grieveson, K. Theuwissen, D. W. McComb, P. D. Nellist, V. Nicolosi, Two-dimensional nanosheets produced by liquid exfoliation of layerd materials, Nicolosi, Science 2011; 331: 568-571.

[29] C. Berger, Z. Song, X. Li, X. Wu, N. Brown, C. Naud, D. Mayou, T. Li, J. Hass, A. N. Marchenkov, E. H. Conrad, P. N. First, W. A. de Heer, Electronic confinement and coherence in patternend epitaxial graphene, Science 2006; 312: 1191–1196.

[30] V. Alzari, D. Nuvoli, S. Scognamillo, M. Piccinini, E. Gioffredi, G. Malucelli, S. Marceddu, M. Sechi, V. Sannab, A. Mariani, Graphene-containig thermoresponsive nanocomposite hydrogels of poly (N-isopropylacrylamide) prepared by frontal polymerization, J. Mater. Chem. 2011; 21: 8727–8733.

[31] E. Ou, Y. Xie, C. Peng, Y. Song, H. Peng, Y. Xiong, W. Xu, High concentration and stable few-layer graphene dispersions prepared by the exfoliation of graphite in different organic solvents, RSC Adv. 2013; 3: 9490-9499.

[32] D. Nuvoli, L. Valentini, V. Alzari, S. Scognamillo, S. B. Bon, M. Piccinini, J. Illescasd, A. Mariani, High concentration few-layer graphene sheets obtained by liquid phase exfoliation of graphite in ionic liquid, J. Mater. Chem. 2011; 21: 3428-3431.

[33] L. Guardia, M. J. Fernández-Merino, J. I. Paredes, P. Solís-Fernández, S. Villar- Rodil, A. Martínez-Alonso, J. M. D. Tascón, High-throughput production of pristine graphene

in an aqueous dispersion assisted by non-ionic surfactants, Carbon 2011; 49: 1653-1662.

[34] S. Perumal, H. M. Lee, I. W. Cheong, High-concentration graphene dispersion stabilized by block copolymers in ethanol. J. Colloid Interface Sci. 2017; 497: 359–367.

[35] M. Z. Rahman, C. W. Kwong, K. Davey, S. Z. Qiao, 2D phosphorene as a water splitting photocatalyst: fundamentals to applications. Energy Environ. Sci. 2016; 9: 709–728.

[36] L. Wang, W. Z. Wang, Graphene/semiconductor nanocomposites: preparation and application for photocatalytic hydrogen evolution. Int. J. Hydrog. Energy 2012; 37: 3041–3047.

[37] X. Y. Yang, C. Salzmann, H. H. Shi, H. Z. Wang, M. L. H. Green, T. C. Xiao, The role of photoinduced defects in TiO_2 and its effects on hydrogen evolution from aqueous methanol solution, J. Phys. Chem. 2008; 112: 10784–10789.

[38] K. Maeda, K. Domen, Photocatalytic water splitting: recent progress and future

challenges, J. Phys. Chem. Lett. 2010; 1: 2655–2661.

[39] T. Kawai, T. Sakata, Photocatalytic hydrogen production from liquid methanol and water, J. Chem. Soc. Chem. Commun. 1980; 15: 694–695.

[40] J. Chen, D. F. Ollis, W. H. Rulkens, H. Bruning, Photocatalyzed oxidation of alcohols and organochlorides in the presence of native TiO_2 and metallized TiO_2 suspensions. Part (II): photocatalytic mechanisms, Water Res. 1999; 33: 669–676.

[41] M. Lotya, Y. Hernandez, P. J. King, R. J. Smith, V. Nicolosi, L. S. Karlsson, F. M. Blighe, S. De, Z. Wang, I. T. McGovern, G. S. Duesberg, J. N. Coleman. Liquid Phase Production of Graphene by Exfoliation of Graphite in Surfactant/Water Solutions, J. Am. Chem. Soc. 2009; 131: 3611-3620.

[42] A. Eckmann, A. Felten, A. Mishchenko, L. Britnell, R. Krupke, K. S. Novoselov, C. Casiraghi, "Probing the nature of defects in graphene by Raman spectroscopy", NanoLett 2012; 12 (8): 3925-3930.

[43] Y. H. Ng, I. V. Lightcap, K. Goodwin, M. Matsumura, P. V. Kamat, "To what extent do graphene scaffolds improve the photovoltaic and photocatalytic response of TiO_2

nanostructured films?", J. Phys. Chem. Lett. 2010; 1(15): 2222-2227.